Journal of the Nigerian Association of Mathematical Physics
Volume 48 (*Sept. & Nov., 2018 Issue*), pp227 –232

TOPOGRAPHIC PHASE BOUNDARY SHIFTS AND SATURATION FOR ANISOTROPIC ION STRAGGLE DURING SPUTTER ETCHING

[*]Emmanuel O. Yewande and [†]Raphael O. Akande

[*]Theoretical Physics Group, Department of Physics, Faculty of Science, University of Ibadan, Ibadan, Nigeria.
[†]Theoretical Physics Group, Mountain Top University, Ogun State, Nigeria.

Abstract

Surfaces sputtered by ion beam bombardment have been known to exhibit patterns whose behaviour is modeled with stochastic partial differential equations. A widely accepted model is the Cuerno-Barabasi model which is robust in its predictions of sputtered surface morphologies. An understanding of the factors responsible for such surface topographies can be achieved by using scaling arguments on the stochastic model. For such explanations, knowledge of the coefficients is crucial. The more so since these vary with different materials, the sputtering process itself generates non-equilibrium surfaces within some finite timescale, and the implication of recent results of surface topographies unexplained by the continuum theory. We calculate and study these coefficients as functions of the sputtering parameters for yet unreported cases of anisotropic ion energy distribution within the sputtered material. Consequently, we present phase diagrams for the significant case of anisotropic ion straggle. We observe shifts in the phase boundaries when the collision cascade geometry rotates, and we also found saturation behavior in the diagrams; in which case the boundaries become independent of the penetration depths. Our results indicate a possible origin of yet unexplained nanodot topographies arising from oblique incidence ion etching of amorphized surfaces.

***Keywords*:** Sputtering, surface morphology, stochastic partial differential equations, continuum theory.

I. INTRODUCTION

Surface sputtering is a process by which materials are removed from the surface of a solid through the impact of energetic particles. There are many sputtering techniques, some of which are for industrial uses. It is a widely applicable technology with remarkable level of sophistication. Sputtering can be used for surface analysis, depth profiling, surface cleaning, micromachining, deposition, surface coating, semiconductor doping, etching, magnetic storage technology, design of nanostructures on a surface and many more [1–4]. The sputtering process creates patterns on the surface at nanometer length scales; hence there is the need to study the surface morphology for knowledge and control of the pattern of these nanostructures exhibited on the surface when it is sputtered. The periodic ripple patterns observed for off-normal incidence sputtering were found to have either of two orientations, depending on the angle of incidence of the impinging energetic ions bombarding the surface [1,5–9]. The ripples are oriented perpendicular to the projection of the ion-beam direction onto the surface plane for small incidence angles, whereas they are oriented parallel to this projection for grazing angles. However, a number of experiments on surface sputtering have observed only a kinetic roughening of the surface, or nanodots, instead of the periodic ripple patterns observed by others [10–15]. Bradley and Harper (BH) were the first to theoretically account for the ripple morphology on amorphous substrate using the linear continuum theory, [16] which entails the theoretical modeling of the surface as a continuum of points whose evolution with time is governed by a deterministic partial differential equation. Their theory provides an understanding of ripple formation and dependence of orientation on ion incidence, but predicts an exponential increase of the ripple amplitude. Experiments, however, observed rough surfaces at larger lengthscales, and a saturation of the surface width [10,11]. An improvement of the linear BH theory is the widely acceptable Cuerno-Barabasi (CB) model which is robust in its predictions of sputtered surface morphologies [4,17]. CB model is a stochastic nonlinear

Corresponding Author**:** Emmanuel O.Y., Email: eo.yewande@ui.edu.ng, Tel: +2347066577984, +2348131597032 (ROA)

continuum model which considers nonlinearities in addition to the linear theory. CB derived this stochastic non-linear equation that mimics the surface evolution with respect to time, by working in the laboratory frame of reference, such that the coefficients appearing in the equation are functions of the actual experimental sputtering parameters. An understanding of the factors responsible for such surface topographies predicted by CB can be achieved by using scaling arguments on the stochastic model based on the relative signs of the coefficients; which are the weighting factors in the continuum model [17]. However, experiments by Fackso and co-workers on normal incidence sputtering of GaSb [18] and Si [12,19] observed nanodots instead of ripple morphologies or kinetic roughening. Moreover, recent results of the discrete theory in [20] and [21], from Monte Carlo simulations of the time evolution of the discretized surface, predicts the presence of such nanodots for oblique incidence sputtering as well. This has been recently confirmed by experiments [15]. Much is still unclear about the continuum theoretical explanations of these recent topographies.

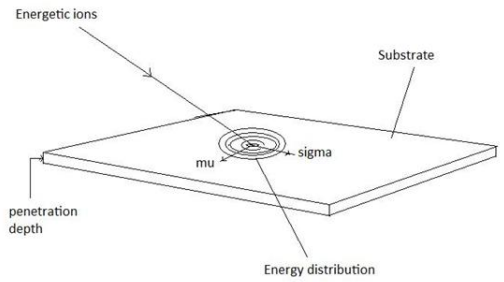

FIG. 1.A schematic diagram of the ion sputtering process.

Thus, knowledge of the surface topographic weighting factors, of the stochastic partial differential equation that describes the surface evolution and their comparative analysis is crucial for an understanding and explanation of the predicted surface topographies and morphology and for knowledge of how these differ fromthe continuum theory predictions. Since the continuum theory calculations have, however, not yet been performed for values of the sputtering parameters of the order of those used in the simulations, it is crucial that this be done in order to ascertain whether, among other things, the nanodots predicted and observed for oblique incidence sputtering constitute a breakdown of the theory.

Hence, in this paper we calculate and comparatively study these sputter coefficients as functions of the sputtering parameters for the case of anisotropic distribution of the energy of the impinging ion within the sputtered material. In which case, we have performed calculations for values of the order of those in the simulations. But, in this first instance, we restrict ourselves mainly to a comparison of the relative strengths of the anisotropic cascade parameters.Our results indicate shifts and saturation of phase boundaries due to the relative strengths of the perpendicular cascading indicators, and suggests a possible origin of yet unexplained nanodot topographies arising from oblique incidence ion etching of amorphized surfaces.

The rest of this paper is organized as follows. In the next section we discuss the linear and the nonlinear continuum theory. In section III, we present and discuss our results of the phase boundaries for the yet unreported anisotropic cases. Finally, we give our conclusions in section IV.

II. CONTINUUM THEORY

For clarity in what follows we provide a schematic diagram, of the ion bombardment of the substrate in a sputtering process, above in Fig. 1. The linear theory of BH[16], is given as equation 1 while the non-linear theory is given as Eq. 2. Equation 2 is an improvement on equation (1) with the introduction of the non-linear terms.

$$\frac{\partial h}{\partial t} = -\nu_o + \nu_o \frac{\partial h}{\partial x} + \beta_x \frac{\partial^2 h}{\partial x^2} + \beta_y \frac{\partial^2 h}{\partial y^2} - D\nabla^2(\nabla^2 h) \dots \dots \dots \dots \dots \dots \dots \dots \dots \dots (1)$$

$$\frac{\partial h}{\partial t} = -\nu_o + \gamma \frac{\partial h}{\partial x} + \nu_x \frac{\partial^2 h}{\partial x^2} + \nu_y \frac{\partial^2 h}{\partial y^2} + \frac{\lambda_x}{2}\left(\frac{\partial h}{\partial x}\right)^2 + \frac{\lambda_y}{2}\left(\frac{\partial h}{\partial y}\right)^2 - D\nabla^2(\nabla^2 h) + \eta \dots (2)$$

$h$is the surface height at position $r, (x, y, z)$and time t;ν_o is the erosion velocity of a flat surface. β_x(or ν_x) is the surface tension coefficient along the x direction, which accounts for the instability created by the sputtering process in which surface depressions (troughs) are eroded in preference to protrusions (crests). $\lambda_x$is the nonlinear coefficient along the x direction, which arises as an improvement of the linear theory to account for the stability of the ripple amplitude and other nonlinear effects observed in experiments. $D$is the surface diffusion coefficient, which takes the thermal hopping of surface atoms into consideration; such migration of surface atoms is the counteracting process tending to restore the surface tension instabilities. The surface patterns observed arises from the right balance of the interplay between the surface tension instabilities arising from the erosion process and the stabilizing effects of surface diffusion. $\eta$is the noise term representing the random nature of the sputtering of surface material; it is taken to be a random variable with a Gaussian distribution and zero mean.

The difference between β_x and ν_x is that the former is a function of the local sputtering parameters in the local surface frame of reference, whereas the latter is a function of the experimental sputtering parameters in the laboratory frame of reference. Thus, apart from equation (2) being a more realistic theoretical picture of the sputtering process, it is also the most relevant in our investigations here for direct comparison with the experimental conditions and, hence, results. The coefficients occurring in equation (2) (derived in [17] and [4]) are provided for ease of reference in the rest of this paper as follows:

$$\nu_x = \mathrm{Y}_a \frac{a_\sigma^2}{2\bar{\omega}^3}\left(2a_\sigma^4 sin^4\theta - a_\sigma^4 a_\mu^2 sin^2\theta cos^2\theta + a_\sigma^2 a_\mu^2 sin^2\theta cos^2\theta - a_\mu^4 cos^4\theta\right) \ldots\ldots\ldots (3)$$

$$\nu_y = -\mathrm{Y}_a \frac{a_\sigma^2 cos^2\theta}{2\bar{\omega}} \ldots\ldots\ldots\ldots\ldots\ldots\ldots\ldots\ldots\ldots\ldots\ldots\ldots\ldots\ldots\ldots\ldots\ldots\ldots\ldots\ldots\ldots\ldots\ldots\ldots\ldots\ldots\ldots (4)$$

$$\lambda_x = \mathrm{Y}\frac{cos\theta}{2\bar{\omega}^4}\left[a_\sigma^8 a_\mu^2 sin^4\theta(3 + 2cos^2\theta) + 4a_\sigma^6 a_\mu^4 sin^2\theta cos^4\theta - a_\sigma^4 a_\mu^6 cos^4\theta(1 + 2sin^2\theta)\right] - \bar{\omega}^2\left[2a_\sigma^4 sin^2\theta - a_\sigma^2 a_\mu^2(1 + 2sin^2\theta)\right] - a_\sigma^8 a_\mu^4 sin^2\theta cos^2\theta - \bar{\omega}^4 \ldots\ldots (5)$$

$$\lambda_y = \mathrm{Y}\frac{cos\theta}{2\bar{\omega}^2}\left[a_\sigma^4 sin^2\theta + a_\sigma^2 a_\mu^2 cos^2\theta - a_\sigma^4 a_\mu^2 cos^2\theta - \bar{\omega}^2\right] \ldots\ldots\ldots\ldots\ldots\ldots\ldots\ldots\ldots\ldots\ldots\ldots (6)$$

Where

$a_\sigma = \frac{a}{\sigma}, a_\mu = \frac{a}{\mu}$, $\bar{\omega} = a_\sigma^2 sin^2\theta + a_\mu^2 cos^2\theta$, $\mathrm{Y} = \frac{FEJa}{\sigma\mu\sqrt{2\pi\bar{\omega}}} exp\left(\frac{a_\sigma^2 a_\mu^2 cos^2\theta}{2\bar{\omega}}\right)$

$F$is the ion flux and J is the proportionality constant between the power deposition and the rate of erosion. For convenience we have set FEJ = 1, which implies the coefficients are in units of FEJ. Cuerno and Barabasi presented results of phase diagram calculations for the isotropic case for simplicity and convenience in their introduction of the theory [17]. They found three different scaling regimes defined by the relative signs of the surface tension and nonlinear coefficients. These scaling regimes are applicable to an understanding of the large length scale (of the order of tens of m) topographies as found in experiments in which topographies have been presented for lower resolution of the probe instruments [often atomic force microscopes (AFM) or scanning tunneling microscopes (STM)]. In this paper we have interpreted our results for the anisotropic case in terms of these three scaling regimes when nonlinearities are relevant. Recent work in [22] found a much larger number of possibilities for the anisotropic case. Following Cuerno and Barabasi, the regions to be encountered below are defined by the signs of the linear and nonlinear coefficients as follows:

I:$\nu_x < 0, \nu_y < 0$, $\lambda_x < 0$, $\lambda_y < 0$

II:$\nu_x < 0, \nu_y < 0$, $\lambda_x > 0$, $\lambda_y < 0$

III:$\nu_x > 0, \nu_y < 0$, $\lambda_x > 0$, $\lambda_y < 0$

For regions I and II, orientations of the ripples formed are along the x direction as this presents the highest magnitude of the modulus of the surface tension coefficients. Region III is characterized by orientations along the y direction since in this case $\nu_x > 0$.

III. RESULTS AND DISCUSSION

The results presented here are obtained from numerical computations of the equations of section II for a ranging between 0 and 3, and for values of θ ranging between 0 and 90°; where we obtain a set of values for each of $\nu_x/y$and λ_x/y, and perform a comparative study of their relative signs for the phase plots. We have not considered higher values of a in order to be able to display the saturation behaviour, which we found to depend on a, without considering values of the collision cascade parameters higher than those in the simulations.

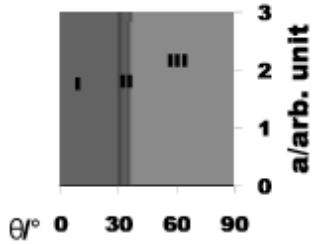

FIG. 2. Phase diagram for the isotropic case σ = μ = 7. The phase boundaries are found to saturate. The regions are as defined and explained in the text.

Shown below are contour plots of the obtained data with which we shall make comparison and then make conclusions. First, we consider higher values of σ and μ that have not yet been reported for the isotropic case introduced in [17], and found the saturation behavior presented in Fig. 2 below for σ = μ = 7.0. As can be seen from this figure, the phase boundaries become independent of the penetration depth, a, for wider ellipsoid of ion straggle within the substrate (see Fig. 1). This implies that,

as values of σ and μ increases the surface ripple patterns and their orientations, as defined by the regions, are observed with the phase boundaries depending on θ and independent of the depth (Fig. 2). In the rest of the paper we present our results for the anisotropic case, $\sigma \neq \mu$. In Figs. 3 and 4, we present the large length scale sputtering behaviour, which consists of the regions I, II, and III as defined above in section II. The short length scale behaviour, discussed below, is presented in Figs. 5 and 6.

A comparison of the phase diagrams of Figs. 2 to 4 indicates that the phase boundaries of region two centered around $\theta \approx 31^o$in Fig. 2 shift to higher values of θ as the relative size of the longitudinal straggle with respect to the lateral straggle parameter μ increase, and to lower $\theta < 31^o$ as the relative size of σ decrease, such that the dominance of the patterns of regions I extend to higher or lower sputtering angles, respectively. With decreasing relative size of σ, we found a shift of region I upwards due to constraints imposed by the increasing dominance of the topography defined by region III.
Thus, surface patterns of region III now dominate almost the entire morphology for experimentally significant incidence angles, and penetration depths. And, topography defined by region I, or region II, is almost irrelevant for common sputtering angles. According to [17] the three regions, found and presented thus far, are applicable to the large length scale properties of the surface morphology, and indicative of the three scaling regions characteristic of sputtered surfaces at such length scales. As pertains to ripple morphologies alone, therefore, there are only two possible regions either one having an orientation that is perpendicular to the other, as explained in section II. Such ripple topographic regions account for the short length scale behaviour. In the rest of the paper, we restrict our- selves to this characterization of the surface morphology in terms of ripple topographies and present results for some anisotropic cases. The regions in the phase diagrams presented below are defined as follows, with the usual orientation characteristics:
I: $\nu_x < \nu_y$, II: $\nu_y < \nu_x$

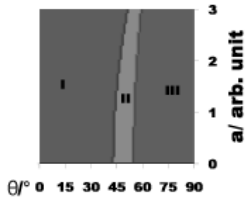

Fig 3a

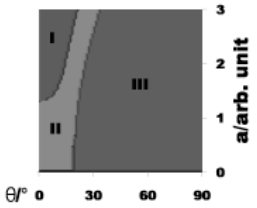

Fig 3b

FIG. 3. Phase diagram for the anisotropic case σ = 3,5, μ = 1.5 [top, Fig 3a]; and vice-versa, Fig 3b.

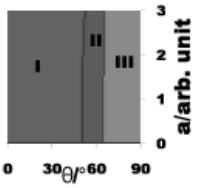

Fig 4a

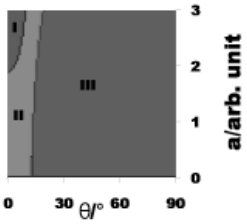

Fig 4b

FIG. 4. Phase diagram for the anisotropic case σ = 6, μ = 2 [top, Fig 4a]; and vice-versa, Fig 4b.

In top part of Figure 5below, we observe that patterns on the surface are more of the orientation defined by region I than that defined by II. For angles less than $\theta_{C1} \approx 54^o$, the ripple orientation is definitely along the x-direction, and for incidence angles greater than $\theta_{C2} \approx 68^o$, the ripple orientation is along the y-direction for this case of anisotropic collision cascade geometry. For angles within the range $\theta_{C1} \leq \theta \leq \theta_{C2}$, the ripple orientation depends on the angle of incidence and penetration depth of the impinging ion within the substrate as in the figure. This interpretation of the result of Fig. 4 applies to Figs. 5 (bottom) and 6, in which cases we also have anisotropic geometries of the ion straggle. We will just note here that the difference is due to the anisotropy, and that changes in the boundaries shown in the figures are due to the relative magnitudes of the cascade parameters as explained above. Note the saturation behavior displayed in the phase diagrams of Fig. 6.

IV. CONCLUSIONS

We have performed phase diagram calculations for practical anisotropic collision cascade parameters yet unreported in order to gain clearer insight into the viewpoint of the continuum theory as regards the origin and theoretical explanation of recent nanodot topographies observed for off-normal incidence sputtering. In any case the anisotropic inclosing geometry of the ion straggle within the substrate is the most likely in reality but unreported as presented here largely because the isotropic cases

that have been reported so far have been mainly for simplicity and ease of presentation of the theory. In this first instance, we have considered the three scaling regions defined by Cuerno and Barabasi in their introduction of the widely acceptable form of the continuum theory. We found shifts in these phase boundaries as the relative magnitude of the collision cascade parameters vary, with saturation for higher values of these parameters. The saturation behaviour has been found for values of the collision cascade parameters higher than the penetration depth. Specifically, we observed that when the relative size of the longitudinal straggle σ is greater than unity, the patterns and large length-scale scaling behaviour of region I dominates while at the same time the phase boundaries straighten from their curved outline until saturation, with increasing σ. On the other hand, when the relative size of σ is less than unity, patterns (and orientation) and scaling of region III dominates while at the same time the influence of region I reduces with increasing μ. The saturation behaviour of the phase boundaries is also found in this case.

This exchange of patterns and orientations strongly suggests a superposition of several patterns and orientation rapidly or gradually (as the case may be) occurring on the topmost surface layer downwards. This may be the factor responsible for the recently reported nanodot topographies predicted for oblique incidence ion sputtering. Hence, while the results are not yet conclusive about nanodot formation, they at least indicate that the nanodot topographies may not constitute a breakdown of the continuum theory.

Through our comparative study of the weighting factors in the stochastic partial differential equation that describes the surface evolution, we have been able to provide these topographic phase diagrams predictive of the large length scale and the short length scale behaviour to be expected in experimental investigations that will almost always obtain anisotropic collision cascades in their surface sputtering. Experimental investigations of the scaling and topographic regimes reported here will constitute an important step in an understanding of the scaling exponents characterizing the large length scale regions.

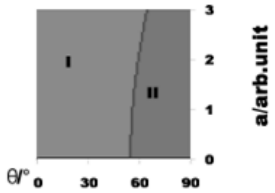

Fig 5a

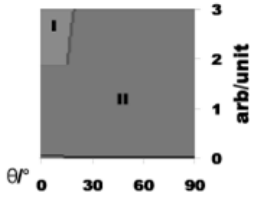

Fig 6a

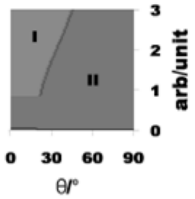

Fig 5b

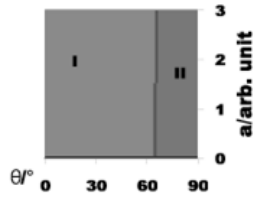

Fig 6b

FIG. 5. Short length scale phase diagram for the anisotropic case σ = 2, μ = 1 [top, Fig 5a]; and vice-versa,Fig5b. The regions observed are as defined in the text.

FIG. 6. Short length scale phase diagram for the anisotropic case σ = 2, μ = 6 [top, Fig 6a]; and vice-versa, Fig 6b.

ACKNOWLEDGMENTS

EOY thanks Alexander Hartmann, Reiner Kree, and Rodolfo Cuerno for discussions while at Gottingen.

References

[1] G. Carter, B. Navinsek, and J. L. Whitton, in Sputtering by Particle Bombardment, Vol. II, edited by R. Behrisch (Springer-Verlag, Heidelberg, 1983) p. 231

[2] E. O. Yewande, Modelling and simulation of surface morphology driven by ion bombardment, PhD dissertation, University of Goettingen, Faculty of Mathematics and Natural Sciences (2006), this is for further details.

[3] J. Munoz-Garcia, L. Vazquez, R. Cuerno, J. A. Sanchez-Garcia, M. Castro, and R. Gago, (2007), ArXiv:0706.2625v1[cond-mat.mtrl-sci]

[4] M. Makeev, R. Cuerno, and A. L. Barabasi, Nucl. Instrum. Methods Phys. Res. B 197, 185 (2002)

[5] E. A. Eklund, E. J. Snyder, and R. S. Williams, Surf. Sci. 285, 157 (1993)

[6] E. A. Eklund, R. Bruinsma, J. Rudnick, and R. S. Williams, Phys. Rev. Lett. 67, 1759 (1991)

[7] S. Habenicht, W. Bolse, K. P. Lieb, K. Reimann, and U. Geyer, Phys. Rev. B 60, R2200 (1999)

[8] S. Habenicht, K. P. Lieb, J. Koch, and A. D. Wieck, Phys. Rev. B 65, 115327 (2002)
[9] J. Krim, I. Heyvaert, C. V. Haesendoncek, and Y. Bruynseraede, Phys. Rev. Lett. 70, 57 (1993)
[10] E. Chason, T. M. Mayer, B. K. Kellerman, D. T. McIlroy, and A. J. Howard, Phys. Rev. Lett. 72, 3040 (1994)
[11] T. M. Mayer, E. Chason, and A. J. Howard, J. Appl. Phys. 76, 1633 (1994)
[12] R. Gago, L. Vazquez, R. Cuerno, M. Varela, C. Ballesteros, and J. M. Albella, Appl. Phys. Lett. 78, 3316 (2001)
[13] S. Facsko, T. Dekorsy, and H. Kurz, Phys. Rev. B 63, 165329 (2001)
[14] F. Frost, A. Schindler, and F. Bigl, Phys. Rev. Lett. 85, 4116 (2000)
[15] B. Ziberi, F. Frost, and B. Rauschenbach, Appl. Phys. Lett. 88, 173115 (2006)
[16] R. M. Bradley and J. M. E. Harper, J. Vac. Sci. Technol. A 6, 2390 (1988)
[17] R. Cuerno and A. L. Barabasi, Phys. Rev. Lett. 74, 4746 (1995)
[18] S. Facsko, T. Dekorsy, C. Koerdt, C. Trappe, H. Kurz, A. Vogt, and H. L. Hartnagel, Science 285, 1551 (1999)
[19] M. Castro, R. Cuerno, L. Vazquez, and R. Gago, Phys. Rev. Lett. 94, 016102 (2005)
[20] E. O. Yewande, A. K. Hartmann, and R. Kree, Phys. Rev. B 73, 115434 (2006)
[21] E. O. Yewande, R. Kree, and A. K. Hartmann, Phys. Rev. B 75, 155325 (2007)
[22] E. O. Yewande, (2010), cond-mat arxive.